gears). (Alternatively, the low-temperature phase might correspond to molecules that are stationary for much longer than the dephasing time of a normal mode of the cluster.) At $T_c$ (244 ± 3 K) these coherently vibrating molecules percolate, forming the first percolating cluster (referred to as the "infinite cluster" in percolation literature), which grows in size with decreasing temperature, eventually encompassing the entire solid. We propose that the 1470 spectrum corresponds to vibrations of the percolating cluster whose constituent molecules vibrate coherently. Because the vibrational time scale is much shorter than rotational time constants, it is the vibrational coherence that is of primary concern here. Nevertheless, the vibrational coupling may result from the ensured molecular alignment that coherent rotation imposes.

According to this model, the dramatic increase in the Raman cross section on going from the high- to the low-temperature forms of solid $C_{60}$ arises from the cooperative Raman scattering by the constituent particles of the percolating cluster (*14*). In its simplest form, cooperative scattering would be characterized by a total Raman cross section that increases as the square of the number of molecules in the cluster. As the cluster grows large, however, the Raman intensity should increase less rapidly with cluster size (*15*). If the percolating cluster is large enough, one would expect saturation to have been reached at $T_c$, beyond which the Raman intensity increases proportionally with cluster size. The average cross section per molecule, however, will be larger than that of an equivalent number of independent scatterers. On the basis of our observations, the average size of the percolating cluster at $T_c$ would be at least ten molecules.

Because no great change in the heat capacity is observed below 249 K (*10*), one must assume that the order-disorder transition is geometric rather than thermodynamic. It is also likely that the incorporation of oxygen decreases the volume per $C_{60}$ molecule in a manner similar to thermal contraction, thereby restricting molecular rotation.

One can make these arguments more quantitative. Frisch *et al.* (*16*) reported the results of Monte Carlo calculations to determine the percolation probability, $P(p)$, as a function of the lattice occupation fraction, $p$. We define $C(p)$ as the fraction of the lattice that belongs to the percolating cluster, that is, $C(p) = pP(p)$. The intensity of the 1470-$cm^{-1}$ line should be proportional to $C(p)$. Using the Monte Carlo data of Frisch *et al.* (*16*) for an fcc lattice, we determined that the value of $p$ at the percolation threshold is $p_c = 0.113$ and that $C(p)$ is well described by the function

$$C(p) = A(p - p_c)^{\theta} \quad (1)$$

with $A = 1.03$ and $\theta = 0.7$ for $p > p_c$ and $C(p) = 0$ for $p < p_c$. Although the relation between $p$ and temperature is unknown, we assume that coherently vibrating molecules correspond to the lower energy state of a two-state system. Hence $p$ is assumed to take the form

$$p(T) = [1 + b \exp(\Delta H/kT)]^{-1} \quad (2)$$

The temperature dependence of the intensity of the 1470-$cm^{-1}$ Raman line, expressed as $Q(T)$, was fit to the above expressions for $C(p)$ and $p(T)$, allowing three parameters to vary: $\Delta H$, $b$, and a scaling constant. A good fit (solid curve in Fig. 2) was obtained over a range of temperatures from approximately 150 K to $T_c$ for the Raman data collected from the three samples studied, with $\Delta H = -4 \pm 1$ kcal $mol^{-1}$ and a value of $b$ consistent with $T_c = 244$ K (when corrected for laser heating). Although $C(T)$ is expected to be nonanalytic at $T_c$, the experimental results show a slight curvature at $T_c$ that varies with sample thickness, suggesting a finite size effect (*16*). A good fit is not expected for temperatures well below $T_c$ because neither the form of $C(T)$ nor the dependence of the Raman intensity on cluster size are known when the cluster is very large. Nevertheless, the sudden change in slope observed at approximately 100 K (Fig. 2) is reproducible and may signal yet another structural change. The value of $\Delta H$ obtained in the fit is reminiscent of the activation energy of the reorientational correlation time for the "ratchet" phase as determined by NMR (*11*).

## REFERENCES


1. H. W. Kroto, J R. Heath, S. C. O'Brien, R. F. Curl, R. E. Smalley, *Nature* **318**, 162 (1985)
2. W. Kratchmer, K. Fostiropoulos, D R. Huffman, *Chem Phys. Lett* **170**, 167 (1990), W. Kratchmer, L D. Lamb, K Fostiropoulos, D. R. Huffman, *Nature* **347**, 354 (1990).
3. *Acc. Chem. Res.* **25** (no. 3) (1992); special issue on Buckmin-sterfullerenes.
4. D. S. Bethune *et al.*, *Chem. Phys. Lett.* **179**, 181 (1991); D. S. Bethune, G. Meijer, W. C. Tang, H J. Rosen, *ibid.* **174**, 219 (1990).
5. D D. Klug, J A. Howard, D. A Wilkinson, *ibid.* **188**, 168 (1992).
6. S. H. Tolbert, A. P. Alivisatos, H. E. Lorenzana, M. B. Kruger, R Jeanloz, *ibid.*, p 163.
7. S J. Duclos, R. C Haddon, S. H. Glarum, A. F. Hebard, K. B. Lyons, *Solid State Commun.*, in press.
8. K. M Creegan *et al.*, *J. Am. Chem. Soc.* **114**, 1103 (1992).
9. F. Diederich *et al.*, *Science* **252**, 548 (1991).
10. P. A. Heiney *et al*, *Phys. Rev. Lett.* **66**, 2911 (1991).
11. R. Tycko *et al.*, *ibid* **67**, 1886 (1991)
12. C. S Yannoni, R. D. Johnson, G. Meijer, D. S. Bethune, J. R. Salem, *J. Phys. Chem.* **95**, 9 (1991); R. Tycko *et al.*, *ibid.*, p. 518.
13. H. E. Stanley, *Introduction to Phase Transitions and Critical Phenomena* (Clarendon, Oxford, 1971).
14. R. H. Dicke, *Phys. Rev.* **93**, 99 (1954); J. C. MacGillivray and M. S. Feld, *Phys. Rev A* **14**, 1169 (1976); S. G. Rautian and B M. Chernobrod, *Sov. Phys. JETP* **45**, 705 (1977).
15. J. Grad, G. Hernandez, S. Mukamel, *Phys. Rev. A* **37**, 3835 (1988).
16. H L. Frisch, J. M Hammersley, J. A Welsh, *Phys. Rev.* **126**, 949 (1962).


9 June 1992; accepted 15 December 1992

# The Nonhelical Structure of Antifreeze Protein Type III

Frank D. Sönnichsen, Brian D. Sykes,* Heman Chao, Peter L. Davies

**Antifreeze proteins (AFPs) are present in the blood of some marine fishes and inhibit the growth of ice crystals at subzero temperatures by adsorption to the ice lattice. The solution structure of a Type III AFP was determined by two-dimensional nuclear magnetic resonance spectroscopy. These measurements indicate that this 66-residue protein has an unusual fold in which eight β strands form two sheets of three antiparallel strands and one sheet of two antiparallel strands, and the triple-stranded sheets are packed orthogonally into a β sandwich. This structure is completely different from the amphipathic, helical structure observed for Type I AFPs.**

The interaction of proteins with solvent water has received much attention, especially the influence of solvent on the stability and folding of proteins (*1*). Less is known about how proteins influence the structure of water. One aspect of this problem is the nature of the interaction near the freezing point of water or at subzero temperatures. Fish AFPs depress the freezing point of water in a noncolligative manner by binding directly to ice crystal nuclei at the interface of ice and water, thereby inhibiting their growth (*2*). The inhibition occurs by preferential adsorption of the

F. D. Sonnichsen and B. D Sykes, Protein Engineering Network of Centres of Excellence and Department of Biochemistry, University of Alberta, Edmonton, Alberta, T6G 2S2, Canada.
H Chao and P. L Davies, Department of Biochemistry, Queen's University, Kingston, Ontario, K7L 3N6, Canada.

*To whom correspondence should be addressed.

AFP to specific prism planes of the hexagonal ice crystal. These antifreeze macromolecules are structurally diverse and have been classified into four different types on the basis of their biochemical properties (*3*, *4*). Similar structure-function relations have been proposed for antifreeze glycoproteins (AFGP) and for Type I AFPs, both of which have simple repetitive sequences (*5*, *6*). An atomic structure of Type I AFP has been determined by x-ray crystallography; the protein forms a long, amphipathic helix (*7*). In contrast, little has been deduced about the structure of the other two types of AFPs (II and III). The only structural information available is that these AFPs are devoid of simple repetitive sequences (*3*, *8*) and of α-helical secondary structure as indicated by circular dichroism measurements (*9*, *10*). Determining the structure of Type II and Type III AFPs will help establish a mechanism for antifreeze activity, determine whether a common structural motif is involved, and improve the understanding of protein-water interactions.

Type III AFPs are produced by fishes of the suborder Zoarcoidei. Numerous isoforms have been sequenced, including eight from ocean pout alone (*3*). Type III AFPs have 62 to 66 amino acids and are heterogeneous at their $NH_2$- and COOH-termini with an overall sequence identity of 50%. The recombinant AFP isoform (rQAE m1.1) selected for structure determination differs from the ocean pout isoform HPLC-12 (*11*) by the inclusion of the $NH_2$-terminal initiating methionine and by the substitution of the COOH-terminal sequence PPA with AA (*12*), an ending used by other AFP Type III isoforms. The antifreeze activity of rQAE m1.1 as measured by thermal hysteresis with a nanoliter osmometer was indistinguishable from that of native HPLC-12 (Fig. 1).

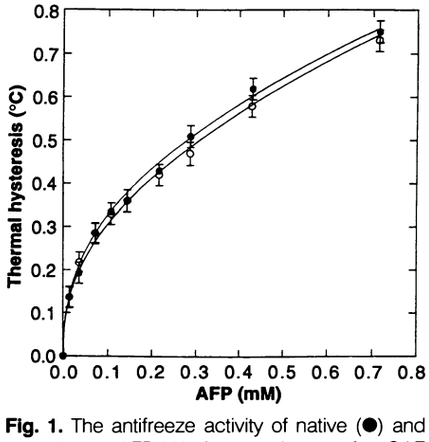


**Fig. 1.** The antifreeze activity of native (●) and recombinant AFP (○). A synthetic gene for rQAE m1.1 was assembled from oligonucleotides and expressed in *Escherichia coli* with the T7 polymerase expression system of Tabor and Richardson (*26*). rQAE m1.1 has the sequence MNQAS-VVANQLIPINTALTLVMMRSEVVTPVGIPAE-DIPRLVSMQVNRAVPLGTTLMPDMVKGYAA (*11*, *12*) and was purified from sonicated *E. coli* by gel permeation chromatography on Sephadex G-75 followed by reversed-phase high-performance liquid chromatography (HPLC). Native QAE-Sephadex–binding isoform HPLC-12 was purified from ocean pout serum by a similar procedure but with the inclusion of cation-exchange chromatography on a CM-52 (Whatman) column to remove other AFP isoforms before reversed-phase HPLC.

We used standard two-dimensional $^1H$ NMR methods to determine the structure of the rQAE m1.1 protein. The portion of the aliphatic region of the 600-MHz $^1H$ NMR spectrum (Fig. 2A) is typical of the high-resolution spectra obtained for this protein. Complete sequential assignments were obtained with the procedure of Wüthrich (*13*, *14*). Secondary structure elements were identified by characteristic nuclear Overhauser effect (NOE) patterns (Fig. 2) in conjunction with information about the φ angle (the dihedral angle around the $C_\alpha$ nitrogen bond) obtained from $J_{NH\text{-}\alpha CH}$ coupling constants (where $J$ is the coupling constant). On this basis, eight short strands of β sheet, several turns, and a loop were identified (Fig. 3). Our data indicate that the loop has an irregular structure from residues 27 to 34 but exhibits NOE connectivities characteristic of a series of turns from residues 35 to 41. The arrangement of the β strands into sheets was established with the use of interstrand NOE connectivities—in particular, cross peaks between α protons of amino acids in adjacent strands (Fig. 2A). Three antiparallel β pleated sheets are formed; two triple-stranded sheets and one two-stranded sheet, which are separated by several turns of various lengths (Fig. 3).

The three-dimensional structure of rQAE m1.1 was obtained from the derived distance and angle information as input into distance geometry (DG) calculations

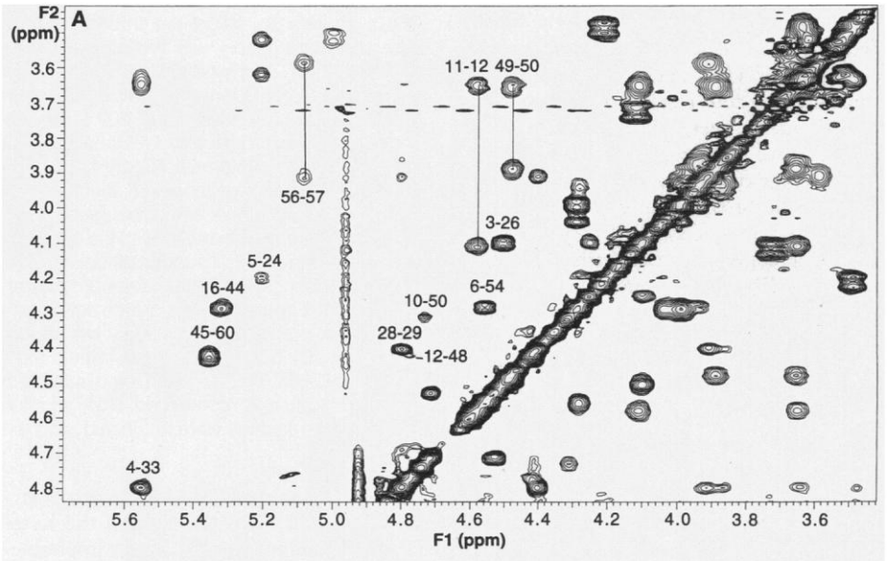


**Fig. 2.** (**A**) Region of two-dimensional $^1H$ NOE spectroscopy (NOESY) NMR spectrum (600 MHz) of rQAE m1.1 at 10°C and pH 4.80. Long-range $d_{\alpha\alpha}$ connectivities (where $d_{\alpha\alpha}$ is the distance between two α proteins) and sequential connectivities involving Pro α carbon protons or δ carbon protons are labeled with residue numbers. F1 and F2, first and second frequency axis, respectively. (**B**) Diagonal plot of interresidue NOE connectivities. Squares above the diagonal represent an NOE between any two protons. Below the diagonal, only backbone-to-backbone NOE cross peaks are represented by diamonds. NMR measurements were performed on a Varian Unity 600 spectrometer with 1 mM solutions of rQAE m1.1 in a solution of 80% $H_2O$ and 20% $D_2O$ or in $D_2O$. Resonance assignments were obtained from total correlation spectroscopy (TOCSY) spectra with 50-, 60-, and 80-ms mixing times, from double quantum-filtered correlated spectroscopy (COSY) data, and from NOESY spectra recorded with 50-, 100-, 150-, and 200-ms mixing times with the use of standard procedures (*13*).

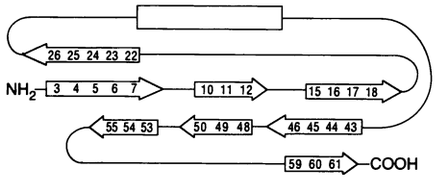


**Fig. 3.** Schematic of the folding pattern of Type III AFP rQAE m1.1. The eight β strands are arranged in three sheets. Arrows and rectangle represent β strands and a series of turns, respectively. Neither the size of the rectangle nor the length of the lines that represent connecting loops are to scale. Numbers in the arrows indicate the residues present in each β strand.

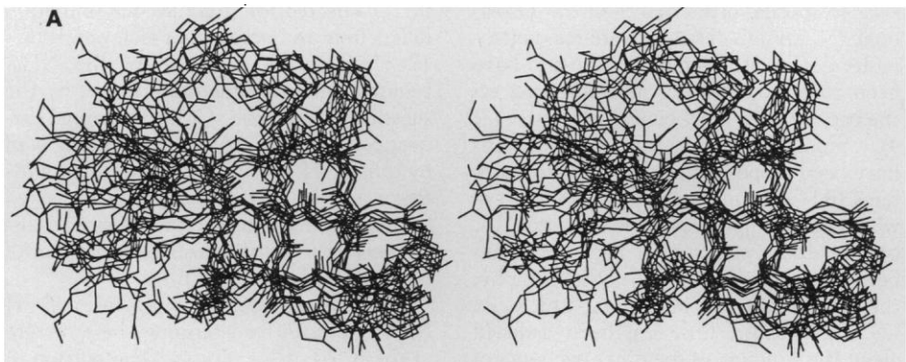


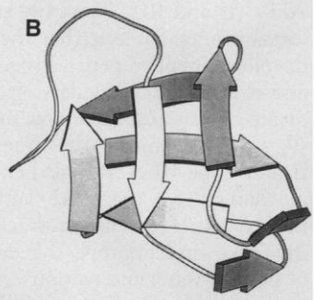


**Fig. 4.** (**A**) Superposition of DG structures of rQAE m1.1 AFP. The structures were generated with Insight II and calculated with DGII and Discover (Biosym, San Diego, California). For NMR structure determination, cross peaks in two-dimensional, 600-MHz $^1$H NOESY spectra (mixing times of 50, 100, and 150 ms) at 10°C and pH 4.80 were integrated. We obtained interproton distances by calibrating the NOE intensities with the use of the Tyr$^{63}$ of proton–ε proton cross peak and classified them as strong, medium, and weak, which corresponded to 2.7, 3.3, and 5 Å upper distance boundaries, respectively. φ angle restraints were used for residues with $J_{NH\text{-}\alpha CH}$ >8 Hz as determined from double quantum-filtered–COSY spectra by fitting the traces of cross peaks to a Lorentzian line shape with the program Jfit (R. Boyko, University of Alberta). Hydrogen bond restraints were used for residues in β pleated sheet regions, where the amide proton was resistant to exchange in $D_2O$ for more than 6 hours at pH 5.8 and 25°C or for more than 5 days at 10°C. In total, 572 NOE (254 intraresidue, 202 sequential, 36 medium-range, and 80 long-range), 16 dihedral angle, and 18 hydrogen bond restraints were introduced in DG calculations with the program DGII (*15*). Of the 25 structures calculated, 20 had residual error function values of 0.3 ± 0.2 kcal/mol, with no remaining distance or dihedral angle violations greater than 0.3 Å or 5 degrees, respectively. The others had errors greater than 0.5 kcal/mol and were disregarded. The structures were subsequently minimized with the use of all restraints, and an average structure was calculated. We obtained the best-fit superposition shown by superimposing the backbone atoms of the β sheet regions and short loops (residues 3 to 26 and 40 to 64) of each DG structure to the average structure. The root-mean-square deviation for the position of backbone atoms is 1.4 ± 0.4 Å. For clarity, the presentation includes ten randomly chosen structures out of the 20 converged structures. (**B**) Schematic of the three-dimensional structure of rQAE m1.1 generated with the program MOLSCRIPT (*27*) with the use of the coordinates of the constrained minimized structure of rQAE m1.1 after 20 converged DGII structures were averaged. The mobile $NH_2$- and COOH-terminal four residues were not included in the display.

with the program DGII (*15*). Twenty-five DG structures were calculated; 20 of them converged onto an identical folding pattern (Fig. 4A). These 20 structures were averaged to show the folding motif (Fig. 4B). The protein folded into a single domain. The two triple-stranded sheets were placed face-to-face, which resulted in a two-layer β sandwich. The alignment of the sheets differed by 90 degrees; they were packed orthogonally (*16*). The two layers were connected by four-residue turns, the short two-stranded sheet, and the loop mentioned above. Although this layered structure is common among proteins (*17*), our results indicate that the folding pattern of rQAE m1.1 is exceptional in respect to its chain topology. This may reflect the fact that Type III AFP sequences are unique—that is, they do not have sequences similar to those of other proteins.

The current mechanism for antifreeze action involves an adsorption-inhibition model that correlates the amphipathic, helical polypeptide properties of AFPs with antifreeze activity (*2*, *18*). In Type 1 AFPs, hydrophilic residues, primarily Thr, Asn, and Asp, are aligned on one face of a long (44 to 64 Å) helix and have been proposed to form hydrogen bonds with the ice surface, whereas the hydrophobic side of the helix is exposed to the solvent, which prevents water from joining the lattice. The adsorption to specific facets of ice has been explained by the spacing of hydrophilic residues, which matches the spacing of the water molecules on the ice crystal surface (*19*–*21*). In particular, a 16.5 Å spacing between polar residues has been implied to be of importance for Type I AFP adsorption.

The globular structure of AFP Type III brings into question some aspects of this mechanism, such as the existence of a universal ice-binding motif. On the basis of our data, Type III AFP (maximum diameter of 35 Å) is much smaller in length than Type I AFP; it has a β-pleated sheet fold and lacks helical character. However, the composition of rQAEm1.1 is unusually hydrophobic (*22*). On the basis of the Kyte-Doolittle parameters (*23*), its hydrophobicity was calculated to be 5.0. Similar values were obtained for Type I AFP, whereas the hydrophobicity of most proteins lies between −6.0 and 0.0. The ratio of hydrophilicity to hydrophobicity for rQAE m1.1 was 0.69. In contrast, the contribution of nonpolar groups to the accessible surface area (*24*) of Type III AFP (63%) falls within the range observed for most proteins (50 to 68%) (*25*) because the folding pattern buries an unusually high proportion of hydrophobic residues in the core. The buried surface therefore consists of 74% nonpolar groups as compared to 60 to 65% for most proteins (*25*). Thus, according to our measurements the protein does not present extended hydrophobic areas to the solvent despite its hydrophobic composition. Two hydrophilic surface areas can be identified: both triple sheets expose six to seven hydrophilic residues to the solvent, which could form hydrogen bonds with the ice surface. The distance between neighboring hydrophilic side chains is approximately 4 or 8 Å, similar to the distance between side chains that are one or two full helical turns apart. This observation is consistent with the adsorption-inhibition mechanism for antifreeze activity (*2*, *18*). However, it is worth noting that these hydrophilic surfaces are on different sides of the protein and are similar to the hydrophilic areas of many other proteins.

Our measurements show that a long linear array of polar side chains as found in Type I AFP is not present in Type III AFP. This could be changed by the association of two or more AFPs when they are in contact with ice or by a partial unfolding of the protein, which would allow both sheets to interact simultaneously with an ice crystal nucleus as well as generate a more amphipathic molecule akin to AFGP and Type I

AFP. However, NMR studies at temperatures near or below the equilibrium freezing point of water do not indicate any intermolecular associations or significant structural changes (*14*).

## REFERENCES AND NOTES


1. G. Otting, E. Liepinsh, K. Wüthrich, *Science* **254**, 974 (1991).
2. J. A. Raymond and A. L. DeVries, *Proc. Natl. Acad. Sci. U.S.A.* **74**, 2589 (1977).
3. P. L. Davies and C. L. Hew, *FASEB J.* **4**, 2460 (1990).
4. C. L. Hew and D. S. C. Yang, *Eur. J. Biochem.* **203**, 33 (1992).
5. R. E. Feeney and Y. Yeh, *Adv. Protein Chem.* **32**, 191 (1978).
6. A. L. DeVries, *Annu. Rev. Physiol.* **45**, 245 (1983).
7. D. S. C. Yang, M. Sax, A. Chakrabartty, C. L. Hew, *Nature* **333**, 232 (1988).
8. P. Hayes, G. K. Scott, N. F. L. Ng, C. L. Hew, P. L. Davies, *J. Biol. Chem.* **264**, 18761 (1989).
9. D. Slaughter, G. L. Fletcher, V. S. Ananthanarayanan, C. L. Hew, *ibid.* **256**, 2022 (1981).
10. V. S. Ananthanarayanan, D. Slaughter, C. L. Hew, *Biochim. Biophys. Acta* **870**, 154 (1986).
11. C. L. Hew *et al.*, *J. Biol. Chem.* **263**, 12049 (1988).
12. Abbreviations for the amino acid residues are: A, Ala; C, Cys; D, Asp; E, Glu; F, Phe; G, Gly; H, His; I, Ile; K, Lys; L, Leu; M, Met; N, Asn; P, Pro; Q, Gln; R, Arg; S, Ser; T, Thr; V, Val; W, Trp; and Y, Tyr.
13. K. Wüthrich, *NMR of Proteins and Nucleic Acids* (Wiley, New York, 1986).
14. F. D. Sönnichsen, unpublished results.
15. T. F. Havel, *Prog. Biophys. Mol. Biol.* **56**, 45 (1991).
16. C. Chothia and J. Janin, *Biochemistry* **21**, 3955 (1982).
17. C. Chothia and A. V. Finkelstein, *Annu. Rev. Biochem.* **59**, 1007 (1990).
18. A. L. DeVries, *Philos. Trans. R. Soc. London Ser. B* **304**, 575 (1984).
19. C. A. Knight, C. C. Cheng, A. L. DeVries, *Biophys. J.* **59**, 409 (1991).
20. D. Wen and R. A. Laursen, *J. Biol. Chem.* **267**, 14102 (1992).
21. K.-C. Chou, *J. Mol. Biol.* **223**, 509 (1992).
22. The calculations were performed with the SEQSEE program written by R. Boyko and D. S. Wishart, University of Alberta, Edmonton, Canada.
23. J. Kyte and R. F. Doolittle, *J. Mol. Biol.* **157**, 105 (1982).
24. The available surface area was calculated with a 1.4 Å probe with the use of Insight II (Biosym, San Diego, CA).
25. S. Miller, J. Janin, A. M. Lesk, C. Chothia, *J. Mol. Biol.* **196**, 641 (1987).
26. S. Tabor and C. C. Richardson, *Proc. Natl. Acad. Sci. U.S.A.* **82**, 1074 (1985).
27. P. J. Kraulis, *J. Appl. Crystallogr.* **24**, 946 (1991).


28. We thank G. Fletcher for the gift of ocean pout serum. Supported by grants from the Medical Research Council of Canada (B.D.S. and P.L.D.), the Protein Engineering Network of Centres of Excellence (B.D.S.), and the Alberta Heritage Foundation for Medical Research (F.D.S.).

2 September 1992; accepted 24 November 1992


# Identification of a Ten–Amino Acid Proline-Rich SH3 Binding Site


Ruibao Ren,* Bruce J. Mayer,* Piera Cicchetti, David Baltimore†



**The Src homology 3 (SH3) region is a small protein domain present in a very large group of proteins, including cytoskeletal elements and signaling proteins. It is believed that SH3 domains serve as modules that mediate protein-protein associations and, along with Src homology 2 (SH2) domains, regulate cytoplasmic signaling. The SH3 binding sites of two SH3 binding proteins were localized to a nine– or ten–amino acid stretch very rich in proline residues. Similar SH3 binding motifs exist in the formins, proteins that function in pattern formation in embryonic limbs of the mouse, and one subtype of the muscarinic acetylcholine receptor. Identification of the SH3 binding site provides a basis for understanding the interaction between the SH3 domains and their targets.**


The SH3 domain, which contains approximately 60 amino acids, is found in a wide variety of proteins. It exists in association with catalytic domains, as in the nonreceptor protein-tyrosine kinases and phospholipase C-γ, within structural proteins such as spectrin or myosin, and in small adapter proteins such as Crk or sem-5 (*1*). SH3 domains are often accompanied by SH2 domains of 100 amino acids that bind to tyrosine-phosphorylated regions of target proteins, frequently linking activated growth factor receptors to putative signal transduction proteins (*1*). The function of the SH3 domain is less well defined. Its presence in a variety of proteins associated with the cytoskeleton implies that it may participate in regulating the cytoskeleton. Deletion or mutation of the SH3 domain generally activates the transforming potential of nonreceptor tyrosine kinases, suggesting that SH3 mediates negative regulation of an intrinsic transforming activity in such proteins (*2*). Studies of vulval development in the nematode, *Caenorhabditis elegans* showed that an SH3-containing protein, Sem5, is central to that process and that the SH3 domains are crucial for the function of Sem5 (*3*).

Two proteins that bind specifically to the SH3 domain of the product of the *abl* proto-oncogene were isolated by screening a λgt11 cDNA expression library with a fusion protein containing glutathione-S-transferase (GST) fused to the SH3 domain of Abl (*4*). One of the proteins, termed 3BP1, contains a region of similarity to GAP-Rho, the guanosine triphosphatase–activating protein for the Ras-related protein Rho. The high-affinity binding site of 3BP1 for the Abl SH3 domain was localized to a 28–amino acid region outside of the domain with similarity to GAP-Rho. We have now localized the SH3 binding sites of 3BP1 and the other Abl SH3 binding protein, termed 3BP2, to a nine– or ten–amino acid stretch very rich in proline residues. The presence of SH3 binding motifs in other known proteins was suggested by a search of the protein sequence data bases and tested in the cases of the formins and a subtype of the muscarinic acetylcholine receptor.

The binding sites for the Abl SH3 do-

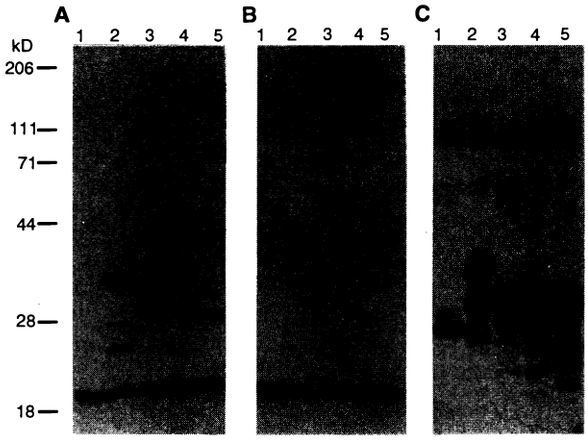


**Fig. 1.** Mapping of the SH3 binding site on 3BP1. Proteins from lysates of bacteria that expressed the GST-3BP1 peptide fusion proteins were probed with biotinylated GST–Abl SH3 fusion protein (0.2 μg/ml) (**A**), biotinylated GST (0.2 μg/ml) (**B**), or antibody to GST (0.5 μg/ml) (**C**). Lane 1, GST (*13*); lane 2, GST-3BP1-64; lane 3, GST-3BP1-28; lane 4, GST-3BP1-22; lane 5, GST-3BP1-10. Numbers on left represent the molecular size in kilodaltons. The antiserum used for detecting GST fusion proteins contains some antibodies to bacterial proteins of large molecular size.


The Rockefeller University, New York, NY 10021.

*The first two authors contributed equally to this work.
†To whom correspondence should be addressed.